HHS Public Access

Author manuscript

Nat Neurosci. Author manuscript; available in PMC 2019 October 31.

Published in final edited form as:

Nat Neurosci. 2019 August ; 22(8): 1276–1288. doi:10.1038/s41593-019-0427-y.

T cells promote microglia-mediated synaptic elimination and cognitive dysfunction during recovery from neuropathogenic flaviviruses

Charise Garber[1,4], **Allison Soung**[1,4], **Lauren L. Vollmer**[1], **Marlene Kanmogne**[1], **Aisling Last**[1], **Jasmine Brown**[1], **Robyn S. Klein**[1,2,3,*]

[1]Department of Internal Medicine, Washington University School of Medicine, St Louis, MO, USA.

[2]Department of Pathology and Immunology, Washington University School of Medicine, St Louis, MO, USA.

[3]Department of Neuroscience, Washington University School of Medicine, St Louis, MO, USA.

[4]These authors contributed equally: Charise Garber and Allison Soung.

Abstract

T cells clear virus from the CNS and dynamically regulate brain functions, including spatial learning, through cytokine signaling. Here we determined whether hippocampal T cells that persist after recovery from infection with West Nile virus (WNV) or Zika virus (ZIKV) impact hippocampal-dependent learning and memory. Using newly established models of viral encephalitis recovery in adult animals, we show that in mice that have recovered from WNV or ZIKV infection, T cell-derived interferon-γ (IFN-γ) signaling in microglia underlies spatial-learning defects via virus-target-specific mechanisms. Following recovery from WNV infection, mice showed presynaptic termini elimination with lack of repair, while for ZIKV, mice showed extensive neuronal apoptosis with loss of postsynaptic termini. Accordingly, animals deficient in $CD8^+$ T cells or IFN-γ signaling in microglia demonstrated protection against synapse elimination following WNV infection and decreased neuronal apoptosis with synapse recovery following

*Correspondence and requests for materials should be addressed to R.S.K. rklein@wustl.edu.

Author contributions

C.G., A.S., and R.S.K. designed the experiments. C.G., A.S., L.L.V., M.K., A.L., and J.B. performed experiments. C.G., A.S., L.L.V., M.K., and R.S.K analyzed the data. R.S.K., C.G., and A.S. wrote the paper. All authors read and edited the manuscript.

Competing interests

The authors declare no competing interests.

Additional information

Supplementary information is available for this paper at https://doi.org/10.1038/s41593-019-0427-y.

Reprints and permissions information is available at www.nature.com/reprints.

Journal peer review information: *Nature Neuroscience* thanks Ryuta Koyama, Susanna Rosi, and the other, anonymous, reviewer(s) for their contribution to the peer review of this work.

Publisher's note: Springer Nature remains neutral with regard to jurisdictional claims in published maps and institutional affiliations.

Reporting Summary. Further information on research design is available in the Nature Research Reporting Summary linked to this article.

Data availability

The data from this study are tabulated in the main paper and supplementary materials. All reagents are available from R.S.K. under a material transfer agreement with Washington University. The data that support the findings of this study are also available from the corresponding author upon request.

ZIKV infection. Thus, T cell signaling to microglia drives post-infectious cognitive sequelae that are associated with emerging neurotropic flaviviruses.

Among the most debilitating consequences of arboviral infections of the CNS is impairment in cognitive function that occurs despite recovery from acute encephalitis. Mosquito-borne infections with flaviviruses, in particular and including WNV and Japanese encephalitis virus, are linked to significant long-term cognitive sequelae, including decreases in psychomotor speed and in verbal and visuospatial learning, which not only persist but also worsen for years after recovery from encephalitis[1]. In addition, the recently emerged and related flavivirus ZIKV may cause a range of neurological complications in adults, including encephalopathy, and meningomyelitis or encephalomyelitis, which may be associated with defects in memory and cognition with unknown long-term outcomes for survivors[2]. In the adult CNS, WNV targets fully differentiated neurons[3], whereas Japanese encephalitis virus targets immature neurons[4] and ZIKV may additionally target microglia[5] and neural progenitors[6] depending on the strain. That recovery from infection with these viruses may all correlate with reduced learning abilities, despite their differential tropism for neural cell subtypes, suggests that events triggered acutely may be generalizable for a broader category of memory disorders.

The formation and consolidation of memories occur primarily in the hippocampus and depends on the integrity of a trisynaptic circuit between the entorhinal cortex, the hippocampal dentate gyrus (DG) and the cornu ammonis (CA). In particular, excitatory connections between CA3 pyramidal neurons support the formation of spatial memories in adult rodents[7]. Accordingly, memory disorders, including those associated with Alzheimer's disease (AD), Parkinson's disease, and post-viral encephalitis cognitive sequelae, are all associated with disruptions in circuit integrity via synapse elimination or neuronal loss within the hippocampus[8–10]. Microglial function is critical for synaptic plasticity and for maintenance of adult neurogenesis within neurogenic niches[11,12]. While mechanisms contributing to hippocampal dysfunction are incompletely understood, recovery from WNV infection clearly involves alterations in the homeostatic functions of microglia and astrocytes. This is because reactive changes in these cells persist for weeks after clearance of the infectious virus, which lead to complement-mediated synapse elimination within the CA3 region[10] and interleukin-1 (IL-1)-mediated inhibition of synaptic repair[13].

Activation of microglia and astrocytes in the acutely infected CNS promotes the parenchymal entry of antiviral T cells, which exert virological control via cytokine-mediated, non-cytolytic mechanisms. T cell cytokines such as IFN-γ may also influence microglial biology. In brain tissues of patients with multiple sclerosis, Parkinson's disease, or AD, infiltrating T cells are found in proximity to activated microglia[14–16], and transition into AD dementia correlates with increased numbers of microglial majorhisto-compatibility complex II $(MHCII)^{+}$ cells[17]. IFN-γ influences social interactions[18], synapse formation[19], neurogenesis[20], and learning and memory[21], primarily through regulatory mechanisms. Thus, IFN-γ-deficient animals show increased rates of hippocampal neurogenesis and synapse formation and hyperconnectivity in the pre-frontal cortex[18,19], all of which are partially reversed by an injection of recombinant IFN-γ into the cerebrospinal fluid. Such

effects suggest that IFN-γ dynamically influences circuit plasticity in adult animals. Resident memory T (T_{rm}) cells, which reside in non-lymphoid tissues at sites of prior antigen exposure, produce IFN-γ to coordinate rapid recall responses following re-challenge[22]. Although there is evidence to indicate that IFN-γ^+ T cells may induce microglial activation, the functional implications of a parenchymal population of T cells that persist in the CNS after clearance of viral infections remain unknown.

In this study, we demonstrate that antiviral T cells that persist within the hippocampus after recovery from flaviviral infection are the most proximal trigger of spatial-learning defects. Using newly established in vivo models of recovery from flaviviral encephalitis caused by either a mutant WNV (WNV-NS5-E218A) or ZIKV (Zika-Dakar virus) infection, we determined that $CD8^+$ T cell-derived IFN-γ is required for microglial activation and impaired spatial learning in the post-infectious CNS. We show that WNV and ZIKV differentially target forebrain regions within adult mice, especially with regard to the hippocampus, which exhibited dramatic differences in neuropathology. However, while both flaviviruses led to the persistence of IFN-γ^+CD8^+ T cells and microglial activation in the hippocampus following recovery, WNV infection was associated with the elimination of presynaptic termini, while ZIKV promoted the loss of neuronal nuclei and postsynaptic termini. Subpopulations of these T cells expressed CD 103, a marker associated with the formation of brain T_{rm} cells, which suggests that the newly formed T_{rm} cells might contribute to these effects. Although IFN-γ receptor (IFNGR)-deficient mice (*Ifngr1*$^{-/-}$) infected with either WNV or ZIKV exhibited no acute defects in CNS virological control, spatial learning was preserved. *Ifngr1*$^{-/-}$ and *Cd8*$^{-/-}$ mice exhibited early recovery of presynaptic termini expressing synaptophysin during recuperation from WNV infection. For ZIKV, *Ifngr1*$^{-/-}$ and *Cd8*$^{-/-}$ mice exhibited decreased neuronal apoptosis with recovery of postsynaptic termini that was most pronounced in the CA regions following viral clearance. Microglial-specific deletion of IFNGR protected mice against spatial-learning deficits and blocked alterations in synapses or neuronal numbers induced during recovery from infection with either virus. These results indicate that T cell and microglial interactions are critical for triggering post-infectious cognitive dysfunction through effects on hippocampal circuitry.

Results

ZIKV preferentially targets the adult hippocampus.

To address the mechanisms of cognitive recovery from neuroinvasive infection with ZIKV, we developed a model of ZIKV infection recovery in adult mice. Direct intracranial inoculation of 8-week-old C57BL/6J (wild-type (WT)) mice with ZIKV-Dakar (Dakar 41525, Senegal, 1984), which shows increased pathogenicity, including higher levels of inflammatory cytokine induction in mice, compared with Asian strains[23], led to weight loss but 100% survival (Fig. 1a,b). This was comparable to our established recovery model of infection with a mutant WNV[10], a strain in which a point mutation in NS5, a nonstructural protein that encodes a 2'-*O*-methyltransferase, prevents viral recognition by tetratricopeptide repeats 1 (IFIT1), which normally acts to block translation of virion-delivered virus-specific RNAs[24]. ZIKV replicated to high levels in the hippocampus and cortex, and, to a lesser extent, in the cerebellum (Fig. 1c). Quantitative PCR (qPCR) analysis of hippocampal tissue

during acute ZIKV infection and recovery demonstrated robust induction of *Cxcl10*, *Tnfa*, and *Il1a* (Fig. 1d), which are molecules known to play important roles during WNV infection of the CNS[25]. Detection of ZIKV or WNV envelope protein (*E*) mRNA via in situ hybridization revealed dramatic differences in viral tropism within forebrain regions. Robust levels of ZIKV *E* mRNA were detected within all regions of the hippocampi of all animals examined. By comparison, *E* mRNA in WNV-infected mice was variably detected in multiple areas throughout forebrain and hindbrain regions (Fig. 1e; Supplementary Fig. 1a,b). Immunohistochemical (IHC) detection of viral proteins within cellular targets of both viruses revealed that both WNV and ZIKV primarily targeted mature neurons (Fig. 1f; Supplementary Fig. 1c,d); however, ZIKV E protein was also detected within $NeuN^+$ cells near the neurogenic subgranular zone of the DG, suggesting that there is additional targeting of immature neurons (Supplementary Fig. 1e,f). These data suggest that direct intracranial infection with ZIKV leads to high viral titers in the hippocampus and induces a neuroinflammatory immune response in animals that survive infection, providing a robust model for recovery from neurotropic viral infection.

ZIKV infection of the adult CNS is associated with loss of neurons.

Expression of cytokines and chemoattractant molecules within the virally infected CNS promotes the recruitment and activation of antiviral T cells, which may persist after viral clearance with unknown consequences[26]. A transcriptional microarray analysis of hippocampal gene expression during recovery of WNV (25 days post-infection (d.p.i.)) indeed identified pathways associated with adaptive immune responses. Genes involved in antigen processing and presentation and in chemokine signaling[10] were identified, which suggests that cytokines and chemoattractant molecules persist beyond acute infection. Indeed, flow cytometry analysis of $CD45^+$ cells in the hippocampus during acute infection and after recovery from ZIKV and WNV encephalitis revealed a large population of infiltrating lymphocytes ($CD45^{hi}CD11b^-$), which were primarily $CD8^+$ T cells, that persisted despite viral clearance (Supplementary Fig. 2). Intraparenchymal T cells and activated astrocytes and microglia were detected robustly at all time points within the hippocampus during recovery from ZIKV infection (Fig. 2a,c), whereas these cells were at the highest levels at 25 d.p.i. with WNV (Fig. 2b,d). Consistent with prior work[10], WNV infection did not lead to neuronal loss in the hippocampus (Fig. 2b,d), although ZIKV infection led to a significant decrease in $NeuN^+$ cells during acute infection that plateaued by 25 d.p.i. (Fig. 2a,c). These data suggest these flaviviruses exert distinct immunopathological effects during recovery.

Antiviral $CD8^+$IFNγ+ T cells associate with microglia in the post-infected hippocampus.

An analysis of infiltrating CNS T cells in mice at 25 d.p.i. with WNV or ZIKV revealed significantly increased percentages of $CD8^+$ T cells expressing the integrin CD103, which has been associated with CNS T_{rm} cell formation[26] (Fig. 2e,f). Percentages of $CD45^{mid}CD11b^+CX3CR1^+CCR2^-$ microglia expressing MHCII, a marker associated with microglial activation that is induced by the T cell cytokine IFN-γ, were also significantly increased (Fig. 2g,h). Consistent with this, the qPCR analysis revealed that hippocampal *Ifng* expression increased following WNV and ZIKV infection, and remained significantly elevated during recovery (Fig. 3a,c). An analysis of IFN-γ-YFP (yellow fluorescent protein)

reporter mice at 25 d.p.i. demonstrated that $CD3^+$ T cells expressed the bulk of IFN-γ in hippocampus at this time point, with $IBA1^+$ microglia representing an additional source (Fig. 3b,d). Flow cytometry analysis of $CD45^+$IFN-γ^+ cells isolated from the hippocampus of IFN-γ-Thy1.1 reporter mice at 25 d.p.i. confirmed that ~15% of the cells were $CD45^{mid}CD11b^+$ microglia, while ~80% were $CD45^{hi}CD11b^-$ lymphocytes, specifically $CD8^+$ T cells (Fig. 3e–g). An analysis of $CD8^+$IFN-γ^+ cells confirmed that a subpopulation of these cells expressed CD103, while detection of NS4B, the predominant CD8 epitope in WNV-infected mice[27], via tetramer staining confirmed virus specificity (Fig. 3f,g; Supplementary Fig. 3). In addition, IFN-γ^+CD8^+ T cells were observed in close proximity to $CX3CR1^+$ microglia at 25 d.p.i. (Fig. 3h,i). An additional flow cytometry analysis of mice at 52 d.p.i. confirmed that $CD8^+$IFN-γ^+ T cells persisted in the hippocampus 1 month after viral clearance (Supplementary Fig. 3). These data show that antiviral T cells reside in the hippocampus following flavivirus infection, and may influence the reactivity of resident neural cell populations through cytokine signaling.

ZIKV-and WNV-infected mice show IFN-γ-mediated deficits in spatial learning post recovery.

While IFN-γ is critical for virological control within the CNS, it is also a dynamic regulator of circuit plasticity[18]. Thus, we hypothesized that IFN-γ signaling between T cells and resident CNS cells may underlie post-infectious cognitive sequelae. Mock, WNV, or ZIKV infection of *Ifngr1*$^{-/-}$ and WT mice did not reveal significant differences in survival, weight loss, or clinical score between these animal models (Supplementary Fig. 4a–f). Consistent with the clinical course, the kinetics of infectious viral replication in most brain regions of the CNS were similar between WT and *Ifngr1*$^{-/-}$ mice following WNV and ZIKV infection (not shown), with the exception of the cerebella in *Ifngr1*$^{-/-}$ animals, for which WNV clearance was significantly delayed, but cleared in both genotypes by 24 d.p.i. (Supplementary Fig. 4g–i). Mock-, WNV-or ZIKV-infected *Ifngr1*$^{-/-}$ and WT mice underwent cognitive behavioral testing 1 month following viral clearance (Fig. 4a). WT mice exhibited spatial-learning deficits on the Barnes maze following WNV infection, as previously described[10,13], as did those recovering from ZIKV infection, while *Ifngr1*$^{-/-}$ mice were protected, showing similar learning curves to mock-infected controls (Fig. 4b,c). To control for alterations in anxiety or movement that could impact performance in hippocampus-dependent tasks, we also performed open-field tests (OFTs). While WNV infection did not alter exploratory or anxiety-like behaviors during the OFT in WT or *Ifngr1*$^{-/-}$ mice (Fig. 4e,g), ZIKV-infected WT and *Ifngr1*$^{-/-}$ mice crossed more lines during the OFT than mock-infected controls (Fig. 4d), but did not show differences in anxiety (Fig. 4f). As this increase in locomotion was observed in both genotypes, this change in behavior is unlikely to explain the difference in the Barnes maze deficits observed between WT and *Ifngr1*$^{-/-}$ mice.

T cell-derived IFN-γ is required to achieve an antiviral state following antigen re-exposure[22], which is an important functional outcome for T_{rm} cell generation. Of interest, we found that there was decreased expression of the T_{rm} cell marker CD103 in a subpopulation of $CD45^{hi}CD11b^-CD8^+$ T cells in the hippocampus of *Ifngr1*$^{-/-}$ animals post recovery from infection compared with WT controls, with minimal CD103 expression in

$CD4^+$ T cells (Supplementary Fig. 5a,b). We also found high levels of CCR2 on a subpopulation of $CD45^{hi}CD11b^-CD8^+$ T cells in the hippocampus of mice that had recovered from infection, the expression of which did not change in the absence of IFN-γ signaling (Supplementary Fig. 5c,d). Importantly, CCR2 expression by $CD3^+$ T cells has been demonstrated in human spinal cord tissue from cases of WNV encephalomyelitis[28]; however, the functional consequence of CCR2 expression by T cells in the CNS remains unknown. Together, these data suggest that IFN-γ signaling negatively affects cognitive recovery from neurotropic viral infections, which is unlikely to be due to differences in clinical disease or virological control.

IFNGR signaling is required for neuronal apoptosis during recovery from ZIKV infection.

Given the dramatic hippocampal targeting and neuronal loss observed following ZIKV infection (Figs. 1 and 2), we determined whether the altered survival of neural cells might underlie spatial-learning deficits. At 25 d.p.i. with ZIKV, *Ifngr1*$^{-/-}$ and $Cd8^{-/-}$ mice exhibited significantly higher levels of NeuN compared with similarly infected WT animals, in which levels were reduced by ~30% of mock-infected controls (Fig. 5a–c). In comparison, WT, *Ifngr1*$^{-/-}$, and *Cd8*$^{-/-}$ mice had similar levels of detection of NeuN following recovery from WNV infection (Fig. 5e–g). Consistent with prior studies[10], we observed no ongoing neuronal loss in WT animals post recovery from WNV infection (Fig. 5e–g). Consistent with the observed loss of $NeuN^+$ cells, TdT-mediated dUTP nick end labeled $(TUNEL)^+$ cells in the DG, CA3, and CA1 regions of the hippocampus of ZIKV-infected WT animals were significantly increased post recovery compared with mock-and ZIKV-infected *Ifngr1*$^{-/-}$ animals post recovery (Fig. 5h). Of note, levels of apoptosis within the DG were considerably lower and more variable than that observed in other hippocampal regions (Fig. 5a,d,h). Within the CA3, which is a region critical for spatial learning, detection of $NeuN^+TUNEL^+$ cells was significantly lower in ZIKV-infected *Ifngr1*$^{-/-}$ and *Cd8*$^{-/-}$ mice compared with similarly infected WT animals after viral clearance (Fig. 5i,j). ZIKV did not target $GAD67^+$ GABAergic neuronal populations, which suggests that the virus may not target interneurons (Supplementary Fig. 6a). In contrast, there were no significant differences in $NeuN^+TUNEL^+$ cells in the hippocampus of WT and *Ifngr1*$^{-/-}$ mice post recovery from mock infection or WNV infection (Fig. 5k). ZIKV also did not alter the number of new neurons born within the DG during recovery from infection, which suggests that impairment in neurogenesis is not a contribution to long-term deficits (Supplementary Fig. 6b). However, increased neuronal loss and apoptosis persisted up to 52 d.p.i. in ZIKV-infected WT mice post recovery compared with mock-and ZIKV-infected *Ifngr1*$^{-/-}$ mice post recovery (Fig. 5l; Supplementary Fig. 6d). These data indicate that WNV and ZIKV lead to differential effects on neurons, including pathology, that contribute to defects in spatial learning.

IFNGR is required for synapse elimination during recovery from WNV infection via IL-1.

Prior studies have demonstrated that WNV infection leads to acute and chronic loss of $synaptophysin^+$ presynaptic terminals, but preservation of $Homer1^+$ postsynaptic terminals, which ceased by 52 d.p.i.[10]. In addition, expression of IL-1β by reactive astrocytes inhibits the recovery of presynaptic termini and is associated with spatial-learning deficits during recovery from WNV infection[13]. Given the synapse recovery observed in *Ifngr1*$^{-/-}$ mice and

the demonstration that IFN-γ influences IL-1β expression[29], we examined levels of this cytokine in WNV-infected *Ifngr1*$^{-/-}$ mice post recovery. Consistent with prior studies[13], we detected increased IL-1β expression by GFAP^{+} astrocytes in the hippocampus of WNV-infected WT mice post recovery, which was significantly decreased in *Ifngr1*$^{-/-}$ animals at 25 d.p.i. (Fig. 6a). As previously reported[10], WNV-infected WT animals showed decreased synaptophysin^{+} presynaptic terminals within the CA3 at 7 and 25 d.p.i., while WNV-infected *Ifngr1*$^{-/-}$ and *Cd8*$^{-/-}$ animals demonstrated limited evidence of synapse elimination at either time point (Fig. 6b,c; Supplementary Fig. 6e). This result suggests that IFNGR is required for synapse elimination during WNV infection. In contrast, and consistent with acute and chronic loss of NeuN^{+} perikarya, ZIKV infection led to loss of Homer1^{+} post-synaptic terminals in WT and *Ifngr1*$^{-/-}$ animals at 7 d.p.i., with preservation of synaptophysin $^{+}$ and vGlut^{+} presynaptic terminals (Supplementary Fig. 6c,f,g). ZIKV-infected WT animals continued to exhibit decreased numbers of Homer1^{+} postsynaptic terminals within the CA3 at 25 and 52 d.p.i., while ZIKV-infected *Ifngr1*$^{-/-}$ animals exhibited recovery of postsynaptic termini by 52 d.p.i. (Fig. 6d,e). ZIKV-infected WT and *Ifngr1*$^{-/-}$ animals also both displayed significantly increased IL-1β expression by GFAP^{+} astrocytes in the hippocampus compared with mock-infected controls post recovery (Supplementary Fig. 7a). Of note, IL-1β expression was not detected within IBA1^{+} cells at 25 d.p.i. (not shown). These data suggest that persistent alterations in postsynaptic termini contribute to spatial-learning deficits in ZIKV-infected mice independent of IL-1β signaling.

IFNGR signaling potentiates microglial engulfment of postsynaptic termini and perikarya in ZIKV-infected animals.

Phagocytic roles for microglia are well established and include removal of both apoptotic newborn cells in the neurogenic niche of the hippocampus and non-apoptotic TBR2^{+} neural progenitors in the developing cerebral cortex, in addition to synapse pruning and elimination, the latter of which requires the upregulation of markers of microglial activation[30]. We therefore wondered whether T cell-derived IFN-γ signaling is required for synapse elimination or neuronal loss following WNV or ZIKV infection, respectively, via specific effects on microglia. Indeed, both WNV and ZIKV infection led to increased expression of IBA1 at 25 d.p.i. in WT mice, which did not occur in similarly infected *Ifngr1*$^{-/-}$ animals (Fig. 7a,b). Importantly, no differences in numbers of CD45^{hi}CD11b $^{+}$CX3CR1^{+}CCR2^{-} microglia cells or expression of TMEM119, a recently described homeostatic marker for microglia, were observed in WNV-and ZIKV-infected WT and *Ifngr1*$^{-/-}$ animals post recovery (Supplementary Fig. 7b–e). This result is consistent with prior data demonstrating that viral infections do not promote microglial proliferation[10]. Flow cytometry analysis of CD45^{mid}CD11b^{+}CX3CR1^{+}CCR2^{-} microglia revealed increased expression of MHCII in WNV-and ZIKV-infected WT animals post recovery; this increased expression was significantly attenuated in *Infgr1*$^{-/-}$ animals (Supplementary Fig. 7f,g). This finding confirms that IFN-γ contributes to microglial activation in the post-infectious CNS. Three-dimensional reconstructions of IBA1^{+} cells from sections of ZIKV-infected mice at 25 d.p.i. revealed Homer1^{+} puncta (Supplementary Video 1) and NeuN^{+} nuclei (Supplementary Video 2) within microglia. Colocalization of Homer1 or NeuN, lysosomal-associated membrane protein 1 (LAMP1), and IBA1 revealed increased numbers of postsynaptic termini within the lysosomes of IBA1^{+} cells, which were significantly reduced

in *Ifngr1*$^{-/-}$ mice at 25 d.p.i. (Fig. 7c–f). These data suggest that microglia may be critically involved in responses to T cell-derived IFN-γ that drive cognitive impairment after infection with either WNV or ZIKV.

Microglial-specific deletion of IFNGR protects animals against spatial-learning defects.

Given the shared alteration in microglial activation observed in both WNV-and ZIKV-infected animals post recovery in the absence of IFN-γ signaling, we utilized a conditional deletion paradigm to determine whether IFN-γ signaling within microglia of mice post recovery was responsible for the observed spatial-learning deficits. *Cx3cr1*^{CreER}*Ifngr*$^{fl/fl}$ (referred to as Cre^{+}hereafter) animals and *Cx3cr1*^{CreER}*Ifngr*$^{fl/fl}$ (referred to as Cre^{-} hereafter) litter-mate controls were mock-infected or infected with WNV or ZIKV, and then treated with tamoxifen 1 week after infectious viral clearance (at 19 and 21 d.p.i.). Animals were allowed to recover for 3 weeks to achieve specific deletion of *Ifngr* in long-lived microglia while allowing time for short-lived CX3CR1-expressing myeloid populations to turnover[31] (Supplementary Fig. 8a–d), at which time cognitive behavior testing was performed (Fig. 8a). Similar to WT animals, tamoxifen-treated Cre^{-} animals displayed significant spatial-learning deficits on the Barnes maze following WNV and ZIKV infection (Fig. 8b,c). In contrast, tamoxifen-treated Cre^{+} animals performed similarly to mock-infected controls (Fig. 8b,c). OFTs confirmed no differences in locomotor activity or anxiety between experimental groups, with the exception of an increase in activity in ZIKV-infected WT animals, as previously shown (Fig. 8d–g). Importantly, microglial-specific deletion of *Ifngr* after viral clearance was sufficient to prevent elimination of synaptophysin^{+} presynaptic termini and neuronal apoptosis in WNV-and ZIKV-infected mice, respectively (Fig. 8h,i). A lack of increased microglial MHCII expression was also observed in WNV-and ZIKV-infected Cre^{+} mice post recovery (Supplementary Fig. 8e,f), confirming that IFN-γ signaling in microglia during recuperation promotes their continued activation. Together, these data suggest that IFN-γ signaling in microglia contributes to microglial activation and spatial-learning deficits following clearance of infectious WNV and ZIKV from the CNS.

Discussion

Antiviral T cells persist within the CNS for months to years after neurotropic viral infections[26]. The extent to which these tissue-resident cells impact on normal brain function is unclear; however, studies of acutely infected mice suggest that CD8^{+} T cells may damage neuronal structures, such as dendrites, during viral clearance[32]. Here, we developed a novel murine model to evaluate mechanisms of cognitive decline following adult ZIKV infection. We found that ZIKV preferentially targets and induces the loss of neurons throughout the hippocampus, which was also associated with the loss of postsynaptic Homer1^{+} termini. In contrast, the related WNV, which infects neurons throughout the CNS, led to elimination of synpato-physin^{+} presynaptic termini, which was most pronounced within the CA3 region of the hippocampus, as previously described[10,13]. Survival after infection with either virus was associated with the recruitment of antiviral CD4^{+} and CD8^{+} T cells, the latter of which persisted in the virus-cleared CNS, expressed CD103, and became a predominant source of IFN-γ. While IFN-γ^{+}CD4^{+} T cells also persisted, targeted deletion of IFN-γ signaling or CD8 was sufficient for reversing the effects of WNV and ZIKV infection on synapses and

apoptosis, respectively. IFN-γ signaling was required for synapse elimination during WNV infection and for the loss of neuronal cell bodies and recovery of synapses after ZIKV infection. Levels of IFN-γ remained elevated after viral clearance, and IFN-γ signaling was required for microglial activation and cognitive dysfunction during recovery from infection with either virus. Microglia-specific deletion of *Ifngr* prevented the development of WNV-or ZIKV-induced hippocampal-dependent learning and memory deficits, suggesting that T cell signaling to microglia is a pivotal event in the development of post-infectious cognitive dysfunction after recovery from flavivirus encephalitis (Supplementary Fig. 9). We used an inducible CX3CR1-Cre line (*Cx3cr1* -Cre^{ERT}) and administered tamoxifen 1 week after viral clearance (~20 d.p.i.), when macrophages are no longer present in the CNS (Supplementary Fig. 2). We therefore designed this experiment to limit the possibility that non-microglial myeloid cells were participating in the process. Nevertheless, as CXC3R1 is not a specific microglial marker, non-microglial cells could possibly contribute to the results obtained.

Infection with ZIKV appears to target the hippocampus in our model. The pathogenesis of ZIKV infection is poorly understood, and there is considerable debate regarding the putative receptors that enable ZIKV infection of various cell types. Several entry receptors, including the innate immune receptor DC-SIGN, the transmembrane protein TIM-1, and TAM receptors (Tyro3, Axl, and Mertk), a family of phosphatidylserine receptors, have been extensively studied for their potential role as flavivirus entry receptors[33]. However, a more recent study investigating different infection routes of ZIKV, including subcutaneous, transplacental, vaginal, and intracranial infections in WT and TAM receptor null mice, showed no difference in viral titers[34]. TAM receptors, at least in mice, are therefore not essential for ZIKV infection, but may play roles in viral tropism. Studies examining *Tyro3* expression in the rodent CNS, however, have demonstrated that it is specifically expressed within the neocortex, especially within the hippocampus[35]. Thus, although Tyro3 is not required for ZIKV infection, the high level of hippocampal expression of this receptor could potentially contribute to ZIKV targeting this CNS region. ZIKV also led to extensive and ongoing neuronal apoptosis in the hippocampus, which was attenuated in the absence of IFN-γ. This is consistent with studies of mice with CNS autoimmune disease, in which IFN-γ is observed to directly induce apoptosis of oligodendrocytes[36]. Alternatively, activated microglia can promote apoptosis by inducing phosphatidylserine exposure and subsequent phagocytosis of neurons by Mertk[37]. The differential extent of neuronal apoptosis and recovery in ZIKV-infected WT, *Ifngr1*$^{-/-}$, and *Cd8*$^{-/-}$ mice supports reports that a threshold number of neurons may be needed to achieve spatial learning[38]. Resolution of neuroinflammation may involve FasL-mediated apoptosis of T cells[39], which may explain the increased numbers of $TUNEL^{+}$ cells that are not neurons.

The persistence of presynaptic termini after ZIKV infection suggests that synaptic boutons of injured axons of hippocampal neurons may be resistant to the rapid loss incurred by other cortical neurons[40]. This also suggests that microglial activation following viral infection does not universally lead to elimination of presynaptic termini, even among closely related virus family members, and that mechanisms leading to microglial-mediated phagocytosis of synapses or neuronal nuclei may be distinct[41]. Elimination of presynaptic termini following WNV infection requires the complement component C3 and its receptor C3aR[10]. Astrocytic

C3 induces C3aR-mediated phagocytosis in a model of AD, but this is attenuated with prolonged exposure to C3 (ref. [42]), which may explain the lack of elimination of presynaptic termini in the setting of the observed robust and persistent ZIKV-induced astrogliosis.

Loss of IFN-γ signaling also led to attenuation of astrocyte activation during recovery from WNV, but not ZIKV, infection. The lack of astrocyte activation in *Ifngr1*$^{-/-}$ animals protected animals against astrocyte IL-1β production[13], which limits synapse repair during recovery from WNV infection[13]. This effect could be caused by a direct loss of IFN-γ signaling in astrocytes, or it could be secondary to the lack of microglial activation[43]. In our model, the latter explanation is more probable given that specific deletion of *Ifngr* in microglia was sufficient to protect animals against spatial-learning deficits, and prior work has demonstrated that in *Csf1r*$^{-/-}$ mice, which lack microglia, lipopolysaccharide injection fails to activate astrocytes[44]. These studies suggest that signaling between microglia and astrocytes critically regulates ongoing neuroinflammation following viral clearance. That spatial learning is preserved in ZIKV-infected *Ifngr1*$^{-/-}$ animals post recovery despite widespread astrocyte reactivity and IL-1β production, which is pathogenic in WNV-infected animals post recovery, adds to the growing body of work demonstrating that heterogeneity in astrocyte reactivity can promote or prevent CNS repair in a disease-specific manner[44].

Although the full spectrum of clinical complications after infection with ZIKV remains unclear, the incidence of neurological manifestations is increasing, including reports of cognitive sequelae[45,46]. Our study also detected increased motor activity in ZIKV-infected mice post recovery. Of interest, neuropsychiatric symptoms, including hyperactivity and hypomania, have been reported in a young adult presenting with ZIKV encephalitis[46]. This finding suggests that ZIKV targeting of the hippocampus may influence cognitive functions beyond spatial learning. Cognitive dysfunction after recovery from WNV infection was first reported in the United States approximately 8 years after its emergence in the New York area[47], and numerous clinical studies since that time have documented persistent psychological and cognitive sequelae following WNV infection[1]. Moreover, the induced cognitive sequelae may worsen over time[1]. In humans, male sex is independently associated with developing neuroinvasive disease and death, especially in older individuals[48]. While no studies have addressed sex differences in cognitive outcomes, higher survival rates of female patients could impact potential findings. In our study, we used both male and female animals in numbers powered to assess cognitive dysfunction but not sex differences. Further studies of both humans and rodents are needed to examine sexually dimorphic features of neurological sequelae after flavivirus encephalitis.

The differential effect of global versus cell-specific deletion of IFNGR on locomotor activity in ZIKV-infected mice suggests that cell-specific roles for this receptor in motor activity may occur during recovery. In addition to microglia, IFNGR is also expressed by astrocytes, neurons, and brain microvasculature, which may each exhibit regional differences in their levels of expression and/or signaling pathways. Given that ZIKV also targets axons in the pyramidal tract (Fig. 1e), it is possible that effects on motor activity are mediated by any of these cell types within this brain region. As microglial-specific deletion of IFNGR abolished hyperactivity, it is possible that IFNGR signaling in microglia specifically limits the effects of the virus on motor function. As the effect was not abolished in mice with global IFNGR

deletion, it is possible that IFNGR signaling of other cell types might override the effects of microglia. Additional studies examining regional and cell-specific differences in IFNGR signaling are needed to determine the mechanism of this effect.

In summary, our studies demonstrate that re-establishing circuit integrity through recovery of lost synapses or neurons is critical for restoring hippocampal function after injury, and identify IFN-γ signaling to microglia as a proximal regulator of this repair in the post-infectious CNS. Given the recent association of herpesviral infections[49] and T cells[50] within the CNS parenchyma of patients with AD, the mechanisms uncovered in our study could have implications for other types of memory disorders.

Online content

Any methods, additional references, Nature Research reporting summaries, source data, statements of code and data availability and associated accession codes are available at https://doi.org/10.1038/s41593-019-0427-y.

Methods

Animals.

Male and female mice (8–10 weeks old) were used for each experiment. C57BL/6J, *Ifngr1*$^{-/-}$, Ifngr$^{fl/fl}$ and CX3CR1-Cre^{ERT} mice were obtained from Jackson Laboratories. Transgenic animals were backcrossed more than ten generations to C57BL/6 mice at Jackson Laboratories. IFN-γ-YFP (C57BL/6 background) and IFN-γ-Thy1.1 (C57BL/6 background) were obtained from H. Shin at Washington Univeristy in St. Louis. CX3CR1^{GFP}CCR2^{RFP} mice were obtained from R. Ransohoff and the Lerner Research Institute and crossed in-house to *Ifngr1*$^{-/-}$ mice to generate *Ifngr1*$^{-/-}$CX3CR1^{GFP}CCR2^{RFP} reporter mice. All experiments followed the guidelines approved by the Washington University School of Medicine Animals Safety Committee (protocol no. 20170064).

Mouse models of WNV infection.

WNV-NS5-E218A and ZIKV-Dakar strains utilized for intracranial infections were obtained from M. Diamond at Washington University in St Louis. WNV-NS5-E218A contains a single point mutation in the gene encoding 2'-*O*-methyltransferase. Mice were deeply anesthetized and intracranially administered 1 X 10^4 plaque-forming units (p.f.u.) of WNV-NS5-E218A or ZIKV-Dakar. Viruses were diluted in 10 μl of 0.5% fetal bovine serum in Hank's balanced salt solution (HBBS) and injected into the third ventricle of the brain with a guided 29-guage needle. Mock-infected mice were intracranially injected with 10 μl of 0.5% in HBSS into the third ventricle of the brain with a guided 29-guage needle. BHK21 cells were used for viral plaque assays to determine stock titers of both viruses (described below).

Measurement of viral burden.

WNV-or ZIKV-infected mice were killed and tissues were collected, weighed, homogenized with zirconia beads in a MagNA Lyser instrument (Roche Life Science) in 500 μl of PBS, and stored at −80 °C until virus titration. Thawed samples were clarified by centrifugation

(2,000 × *g* at 4 °C for 10 min), and then diluted serially before infection of BHK21 cells. Plaque assays were overlaid with low-melting point agarose, fixed 4 days later with 10% formaldehyde, and stained with crystal violet. Viral burden was expressed on a $\log_{10}$ scale as p.f.u. per gram of tissue. During initial development of the adult ZIKV infection and recovery model (Supplementary Fig. 1), viral burden was determined by qPCR with reverse transcription (qRT-PCR). RNA was extracted using a RNeasy Mini kit (Qiagen). ZIKV levels were determined by one-step qRT-PCR on an Applied Biosystems ViiA7 Real-Time PCR system using standard cycling conditions. A standard curve was produced using serial tenfold dilutions of ZIKV RNA, and viral burden was expressed as viral RNA equivalents per gram of tissue.

Immunohistochemistry.

Mice were anesthetized and perfused with ice-cold Dulbecco's PBS (Gibco) followed by ice-cold 4% paraformaldehyde (PFA). Brains were post-fixed overnight in 4% PFA followed by cyroprotection in 30% sucrose (three exchanges for 24 h), then frozen in OCT compound (Fischer). Coronal tissue sections (10 μm) were washed with PBS and permeabilized with 0.1–0.3% Triton X-100 (Sigma-Aldrich). Nonspecific antibodies were blocked with 5% normal goat serum (Sigma-Aldrich) at room temperature for 1 h. To reduce endogenous mouse antibody staining when detecting ZIKV, a Mouse on Mouse kit (MOM basic kit, Vector) was used as per the manufacturer's instructions. Slides were then incubated in primary antibody (described below) or isotype-matched IgG overnight at 4 °C. Following washes in PBS, slides were then incubated in secondary antibodies at room temperature for 1 h, and nuclei were counterstained with 4,6-diamidino-2-phenylindole (DAPI; Invitrogen). Coverslips were applied with ProLong Gold Antifade Mountant (Thermo Fisher). Immunofluorescent images were acquired using a Zeiss LSM 880 confocal laser scanning microscope and processed using software from Zeiss. Immunofluorescent signals were quantified using the software ImageJ.

Antibodies for immunohistochemistry.

The following primary antibodies were used for IHC analyses: WNV (1:100, polyclonal[25]), ZIKV (1:50; gift from M. Diamond (St. Louis, MO), ZV-13), NeuN (1:1,000; Cell Signaling, cat no. 12943S, clone D3S3I), BrdU (1:200; Abcam, cat. no. ab1893, polyclonal), doublecortin (1:125; Cell Signaling, cat. no. 4604S, polyclonal), GFAP (1:250; Thermo, cat. no. 13–0300, clone 2.2B10), IL-1β (1:100; R&D, cat. no. AF-401, polyclonal), CD3 (1:250; R&D, cat. no. MAB4841, clone 17A2), CD11c (1:50; Novus, cat. no. NB110– 97871, clone AP-MAB0806), GFP (1:500; Abcam, cat. no. ab13970, polyclonal), IBA1 (1:200; Wako, cat. no. 019–19741, polyclonal), TMEM119 (1:200; Abcam, cat. no. ab209064, clone 28–3), TUNEL (Roche In situ Cell Death kit Red), and synaptophysin (1:250; Synaptic Systems, cat. no. 101004, polyclonal). Secondary antibodies conjugated to Alexa-488 (Invitrogen, cat. no. A-21206, polyclonal) or Alexa-555 (Invitrogen, cat. no. A-21435, polyclonal) were used at a 1:400 dilution.

Three-dimensional reconstruction of confocal z-stack images.

Confocal z-stack images were taken using a Zeiss LSM 880 laser scanning microscope with Airyscan at ×63 magnification, and consisted of at least eight images. Images were

transformed into three-dimensional reconstruction videos using the image analysis software Volocity 3D image.

RNAscope in situ hybridization.

Mice were anesthetized and perfused with ice-cold PBS. Brains were then immersion-fixed overnight in 4% PFA followed by three exchanges of 30% sucrose for 24 h. Brains were embedded in OCT compound (Fischer) and 10-μm sagittal tissue sections were prepared. RNAscope 2.5 HD Assay-Brown was performed as per the manufacturer's instructions. Probes against WNV and ZIKA mRNA (ACD) were used. Viral tropism was analyzed using a ZEISS Axio Imager Z2 fluorescence microscope.

Flow cytometry.

Cells from the hippocampus and cortex of mice were isolated at indicated d.p.i. and stained with fluorescence-conjugated antibodies (described below) as previously described[13]. Briefly, mice were anesthetized and perfused with ice-cold Dulbecco's PBS (Gibco). Hippocampal and cortex brain tissue were dissected out, minced, and enzymatically digested at room temperature for 1 h with shaking. The digestion buffer contained collagenase D (Sigma, 50 mg ml^{-1}), TLCK trypsin inhibitor (Sigma, 100 μg ml^{-1}), DNase I (Sigma, 100 U $μl^{-1}$), HEPES buffer, pH 7.2 (Gibco, 1 M) in HBSS (Gibco). The tissue was then pushed through a 70-μm strainer and pelleted by a 500 × *g* spin cycle for 10 min. To remove myelin debris, cells were resuspended in 37% Percoll and spun at 1,200 × g for 30 min. Cells were then resuspended in FACS buffer. TruStain fcX anti-mouse CD16/32 (BioLegend, cat. no. 101320, clone 93) was used to block the cells for 5 min at 4 °C, followed by cell surface staining for 15 min at 4 °C. Cells were washed twice in FACS buffer, fixed with 4% PFA, and resuspended in 2% PFA for data acquisition. Data were collected using a Fortessa X-20 instrument and analyzed with the software Flowjo.

Antibodies for flow cytometry.

The following antibodies were used for flow cytometry: CD45 (PE/Cy7, BioLegend, cat. no. 103114, clone 30-F11), CD11b (Brilliant Violet 605, BioLegend, cat. no. 101257, clone M1/70), I-A/I-E (MHC-II, APC/Cy7, BioLegend, cat. no. 107628, clone M5/114.15.2), CD4 (Alexa Fluor 700, BioLegend, cat. no. 100536, clone RM4–5), CD8 (PerCP/Cy5.5, BioLegend, cat. no. 100734, clone 53–6.7), NK1.1 (Brilliant Violet 421, BioLegend, cat. no. 108741, clone PK136), CD103 (APC, BioLegend, cat. no. 121414, clone 2E7), Thy1.1 (PE, BioLegend, cat. no. 202524, clone OX-7), CD119 (IFNGR, Biotin, BD Biosciences, cat. no. 558771, clone GR20), and streptavidin (PE, BD Biosciences, cat. no. 554061).

Behavioral testing.

Animals underwent open-field and Barnes maze testing as previously described[13]. Briefly, mice were given 3 min to explore the Barnes maze platform and to find the target hole. If a mouse did not find the target hole within the test period, it was gently guided in the hole. At the end of a trial, the mice remained in the target hole for 1 min before being placed back into their home cage between trials. Each mouse received two trials per day over the course of five consecutive days. The number of errors (or number of nose pokes over non-target

holes) was recorded. Before Barnes maze testing, animals performed the OFT as a measure of exploratory behavior. Each mouse was given 5 min to explore an empty arena before being placed back into its home cage. Both the Barnes maze platform and the open-field arena were decontaminated with 70% ethanol between trials and/or mice. All trials were video recorded using a camera (Canon Powershot SD1100IS) and scored by experimenters blinded to the treatment conditions.

Statistical analysis.

Unpaired Student's *t*-test or one-way or two-way analysis of variance (ANOVA) with appropriate post-test to correct for multiple comparisons, in which the means of all groups were compared pairwise, were performed as indicated in the figure legends. Prism 7.0 (GraphPad Software) was used for generating graphs and statistical analyses. *P* values of ≤0.05 were considered significant. To determine sample sizes for virological and immunological studies, a power analysis was performed using the following values: probability of type I error = 0.05, power = 80%, fivefold hypothetical difference in mean, and population variance of 25-fold (virological studies) or 12-fold (immunological studies). Sample sizes for behavioral testing experiments were predetermined by the power analysis. For all experiments, animals were randomly assigned to mock, WNV or ZIKV infection. Investigators were blinded to group allocation during data collection and analyses.

Supplementary Material

Refer to Web version on PubMed Central for supplementary material.

Acknowledgements

The authors acknowledge M. Diamond, J. Miner, A. Smith, L. Thackray, and K. Funk for helpful discussions and technical support. They also thank W. Beatty at the Molecular Microbiology Imaging facility at Washington University School of Medicine. This work was supported by NIH grants U19 AI083019, R01 NS052632, and R01 AI101400 to R.S.K.

References

1. Murray KO et al. Survival analysis, long-term outcomes, and percentage of recovery up to 8 years post-infection among the Houston West Nile virus cohort. PLoS One 9, e102953 (2014).
2. Mehta R. et al. The spectrum of neurological disease associated with Zika and chikungunya viruses in adults in Rio de Janeiro, Brazil: a case series. PLoS Negl. Trop. Dis. 12, e0006212 (2018).
3. Shrestha B, Gottlieb D. & Diamond MS Infection and injury of neurons by West Nile encephalitis virus. J. Virol. 77, 13203–13213 (2003). [PubMed: 14645577]
4. Ogata A. et al. Japanese encephalitis virus neurotropism is dependent on the degree of neuronal maturity. J. Virol. 65, 880–886 (1991). [PubMed: 1987378]
5. Lum FM et al. Zika virus infects human fetal brain microglia and induces inflammation. Clin. Infect. Dis. 64, 914–920 (2017). [PubMed: 28362944]
6. Garcez PP et al. Zika virus impairs growth in human neurospheres and brain organoids. Science 352, 816–818 (2016). [PubMed: 27064148]
7. Neunuebel JP & Knierim JJ CA3 retrieves coherent representations from degraded input: direct evidence for CA3 pattern completion and dentate gyrus pattern separation. Neuron 81, 416–427 (2014). [PubMed: 24462102]
8. Hong S. et al. Complement and microglia mediate early synapse loss in Alzheimer mouse models. Science 352, 712–716 (2016). [PubMed: 27033548]

9. Lui H. et al. Progranulin deficiency promotes circuit-specific synaptic pruning by microglia via complement activation. Cell 165, 921–935 (2016). [PubMed: 27114033]
10. Vasek MJ et al. A complement-microglial axis drives synapse loss during virus-induced memory impairment. Nature 534, 538–543 (2016). [PubMed: 27337340]
11. Parkhurst CN et al. Microglia promote learning-dependent synapse formation through brain-derived neurotrophic factor. Cell 155, 1596–1609 (2013). [PubMed: 24360280]
12. Sierra A. et al. Microglia shape adult hippocampal neurogenesis through apoptosis-coupled phagocytosis. Cell Stem Cell 7, 483–495 (2010). [PubMed: 20887954]
13. Garber C. et al. Astrocytes decrease adult neurogenesis during virus-induced memory dysfunction via IL-1. Nat. Immunol. 19, 151–161 (2018). [PubMed: 29292385]
14. Brochard V. et al. Infiltration of CD4+ lymphocytes into the brain contributes to neurodegeneration in a mouse model of Parkinson disease. J. Clin. Invest 119, 182–192 (2009). [PubMed: 19104149]
15. Grebing M. et al. Myelin-specific T cells induce interleukin-1beta expression in lesion-reactive microglial-like cells in zones of axonal degeneration. Glia 64, 407–424 (2016). [PubMed: 26496662]
16. Togo T. et al. Occurrence of T cells in the brain of Alzheimer's disease and other neurological diseases. J. Neuroimmunol. 124, 83–92 (2002). [PubMed: 11958825]
17. Paz J, Yao H, Lim HS, Lu XY & Zhang W The neuroprotective role of attractin in neurodegeneration. Neurobiol. Aging 28, 1446–1456 (2007). [PubMed: 16860906]
18. Filiano AJ et al. Unexpected role of interferon-gamma in regulating neuronal connectivity and social behaviour. Nature 535, 425–429 (2016). [PubMed: 27409813]
19. Kim IJ, Beck HN, Lein PJ & Higgins D. Interferon gamma induces retrograde dendritic retraction and inhibits synapse formation. J. Neurosci. 22, 4530–4539 (2002). [PubMed: 12040060]
20. Li L, Walker TL, Zhang Y, Mackay EW. & Bartlett PF Endogenous interferon gamma directly regulates neural precursors in the non-inflammatory brain. J. Neurosci. 30, 9038–9050 (2010). [PubMed: 20610738]
21. Monteiro S. et al. Absence of IFNgamma promotes hippocampal plasticity and enhances cognitive performance. Transl. Psychiatry 6, e707 (2016). [PubMed: 26731444]
22. Schenkel JM et al. T cell memory. Resident memory CD8 T cells trigger protective innate and adaptive immune responses. Science 346, 98–101 (2014). [PubMed: 25170049]
23. Tripathi S. et al. A novel Zika virus mouse model reveals strain specific differences in virus pathogenesis and host inflammatory immune responses. PLoS Pathog. 13, e1006258 (2017).
24. Daffis S. et al. 2'-O methylation of the viral mRNA cap evades host restriction by IFIT family members. Nature 468, 452–456 (2010). [PubMed: 21085181]
25. Durrant DM, Robinette ML & Klein RS IL-1R1 is required for dendritic cell-mediated T cell reactivation within the CNS during West Nile virus encephalitis. J. Exp. Med. 210, 503–516 (2013). [PubMed: 23460727]
26. Wakim LM, Woodward-Davis A. & Bevan MJ Memory T cells persisting within the brain after local infection show functional adaptations to their tissue of residence. Proc. Natl Acad. Sci. USA 107, 17872–17879 (2010). [PubMed: 20923878]
27. Kaabinejadian S. et al. Immunodominant West Nile virus T cell epitopes are fewer in number and fashionably late. J. Immunol. 196, 4263–4273 (2016). [PubMed: 27183642]
28. Mahad D. et al. Modulating CCR2 and CCL2 at the blood-brain barrier: relevance for multiple sclerosis pathogenesis. Brain 129, 212–223 (2006). [PubMed: 16230319]
29. Eigenbrod T, Bode KA & Dalpke AH Early inhibition of IL-1beta expression by IFN-gamma is mediated by impaired binding of NF-kappaB to the IL-1beta promoter but is independent of nitric oxide. J. Immunol. 190, 6533–6541 (2013). [PubMed: 23667107]
30. Ebner F. et al. Microglial activation milieu controls regulatory T cell responses. J. Immunol. 191, 5594–5602 (2013). [PubMed: 24146044]
31. Goldmann T. et al. Origin, fate and dynamics of macrophages at central nervous system interfaces. Nat. Immunol. 17, 797–805 (2016). [PubMed: 27135602]

32. Kreutzfeldt M. et al. Neuroprotective intervention by interferon-gamma blockade prevents $CD8^+$ T cell-mediated dendrite and synapse loss. J. Exp. Med 210, 2087–2103 (2013). [PubMed: 23999498]
33. Nowakowski TJ et al. Expression analysis highlights AXL as a candidate Zika virus entry receptor in neural stem cells. Cell Stem Cell 18, 591–596 (2016). [PubMed: 27038591]
34. Hastings AK et al. TAM receptors are not required for Zika virus infection in mice. Cell Rep. 19, 558–568 (2017). [PubMed: 28423319]
35. Prieto AL, O'Dell S, Varnum B. & Lai C. Localization and signaling of the receptor protein tyrosine kinase Tyro3 in cortical and hippocampal neurons. Neuroscience 150, 319–334 (2007). [PubMed: 17980494]
36. Ottum PA, Arellano G, Reyes LI, Iruretagoyena M. & Naves R. Opposing roles of interferon-gamma on cells of the central nervous system in autoimmune neuroinflammation. Front. Immunol. 6, 539 (2015). [PubMed: 26579119]
37. Neher JJ et al. Phagocytosis executes delayed neuronal death after focal brain ischemia. Proc. Natl Acad. Sci. USA 110, E4098–E4107 (2013).
38. Nakatomi H. et al. Regeneration of hippocampal pyramidal neurons after ischemic brain injury by recruitment of endogenous neural progenitors. Cell 110, 429–441 (2002). [PubMed: 12202033]
39. Wang X, Haroon E, Karray S, Martina D. & Schluter D. Astrocytic Fas ligand expression is required to induce T-cell apoptosis and recovery from experimental autoimmune encephalomyelitis. Eur. J. Immunol. 43, 115–124 (2013). [PubMed: 23011975]
40. Canty AJ et al. Synaptic elimination and protection after minimal injury depend on cell type and their prelesion structural dynamics in the adult cerebral cortex. J. Neurosci. 33, 10374–10383 (2013). [PubMed: 23785150]
41. Vilalta A. & Brown GC Neurophagy, the phagocytosis of live neurons and synapses by glia, contributes to brain development and disease. FEBS J 285, 3566–3575 (2018). [PubMed: 29125686]
42. Lian H. et al. Astrocyte-microglia cross talk through complement activation modulates amyloid pathology in mouse models of Alzheimer's disease. J. Neurosci. 36, 577–589 (2016). [PubMed: 26758846]
43. Savarin C. et al. Astrocyte response to IFN-gamma limits IL-6-mediated microglia activation and progressive autoimmune encephalomyelitis. J. Neuroinflamm. 12, 79 (2015).
44. Liddelow SA et al. Neurotoxic reactive astrocytes are induced by activated microglia. Nature 541, 481–487 (2017). [PubMed: 28099414]
45. Nicastri E, Castilletti C, Balestra P, Galgani S. & Ippolito G. Zika virus infection in the central nervous system and female genital tract. Emerg. Infect. Dis. 22, 2228–2230 (2016). [PubMed: 27617352]
46. Zucker J. et al. Zika virus-associated cognitive impairment in adolescent, 2016. Emerg. Infect. Dis. 23, 1047–1048 (2017). [PubMed: 28518023]
47. Sejvar JJ The long-term outcomes of human West Nile virus infection. Clin. Infect. Dis. 44, 1617–1624 (2007). [PubMed: 17516407]
48. Borchardt SM, Feist MA, Miller T. & Lo TS Epidemiology of West Nile virus in the highly epidemic state of North Dakota, 2002–2007. Public Health Rep. 125, 246–249 (2010). [PubMed: 20297751]
49. Readhead B. et al. Multiscale analysis of independent Alzheimer's cohorts finds disruption of molecular, genetic, and clinical networks by human herpesvirus. Neuron 99, 64–82 e67 (2018). [PubMed: 29937276]
50. Unger MS et al. Doublecortin expression in CD8+ T-cells and microglia at sites of amyloid-beta plaques: a potential role in shaping plaque pathology? Alzheimers Dement. 14, 1022–1037 (2018). [PubMed: 29630865]

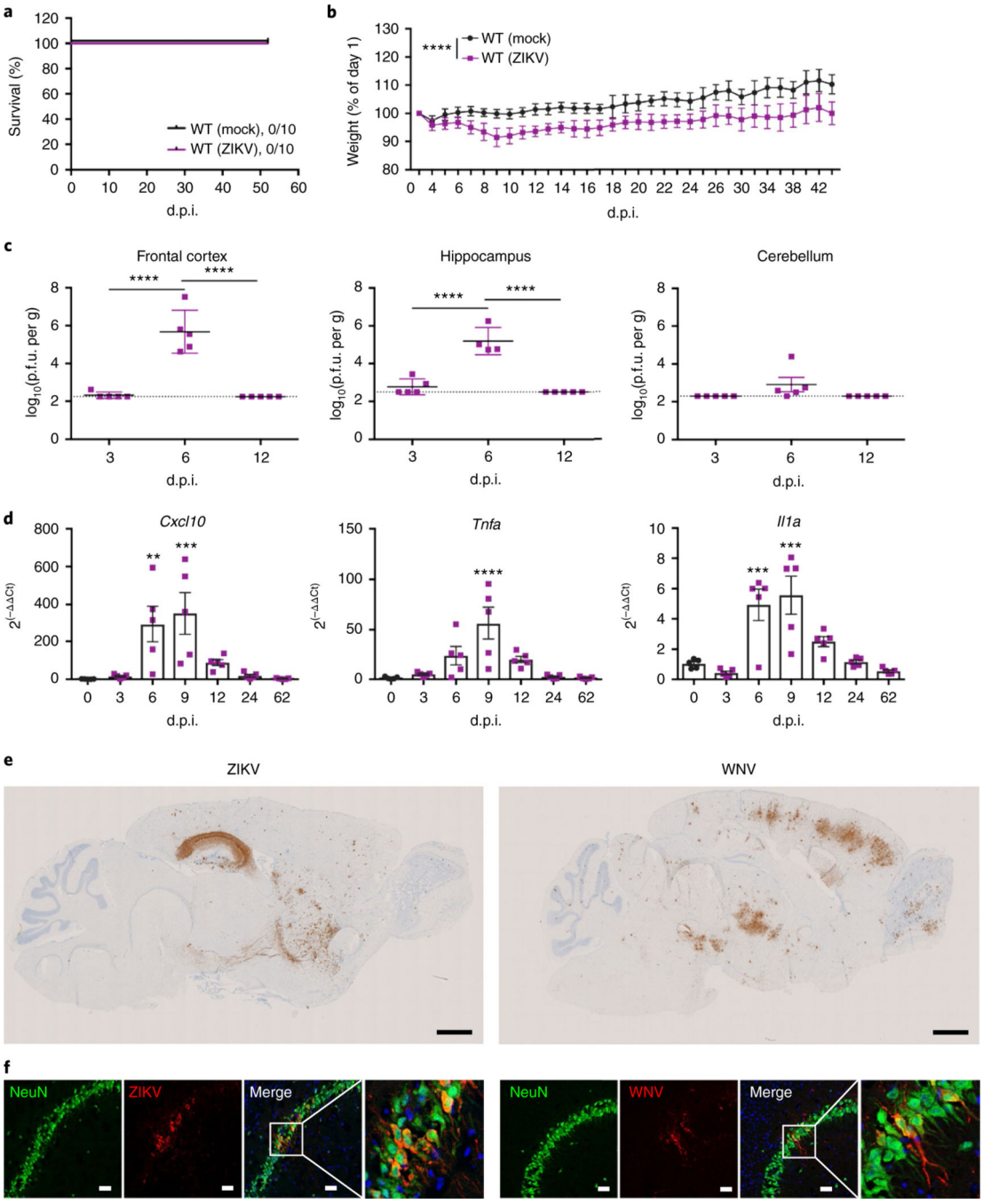

Fig. 1 |. ZiKV targets the hippocampus.

a-d, Establishing a mouse model of adult ZIKV infection and recovery. **a**, ZIKV infection did not cause lethality in adult mice. **b**, ZIKV infection led to weight loss, expressed as the percentage of day 0 body weight. Data were pooled from two independent experiments (n = 10 mice per group; P< 0.0001). **c**, ZIKV replicated in the CNS of WT mice. Viral burden was quantified via standard plaque assays (n = 5 mice per group; P = 0.0001 for the frontal corext and hippocampus). P.f.u., plaque-forming units. **d**, ZIKV infection induced cytokine responses in the hippocampus. qPCR analysis of indicated mRNA isolated from the

hippocampus at the indicated d.p.i. (n = 5 mice per group). *Cxcl10* (left to right), $P = 0.0048$ and 0.0007; *Tnfa*, $P < 0.0001$; *Il1a* (left to right), P = 0.0010 and 0.0002. **e,f**, ZIKV and WNV target different regions of the CNS during acute infection, but similarly infect mature neurons in the hippocampus. **e**, In situ hybridization for viral RNA at 7 d.p.i. revealed dramatic differences in the neurotropism of WNV and ZIKV. ZIKV consistently targeted the hippocampus, with sparse infection of the cortex and striatum. Conversely, WNV RNA was present throughout the CNS, including the olfactory bulb, cortex, hippocampus, and cerebellum. Representative images shown ($n = 4$ mice per group) here, with additional images shown in Supplementary Fig 1. Scale bars,1,000 μm. **f**, ZIKV and WNV target mature neurons in the hippocampus. Representative immunostaining of the CA3 region of the hippocampus for NeuN (green), viral antigen (red), and DAPI (blue). Data are representative of one independent experiment. Scale bar, 20 μm. For **b-d**, data represent the mean ± s.d. and were analyzed by two-way (**b**) or one-way (**c** and **d**) ANOVA, and corrected for multiple comparisons. $^{**}P < 0.005$, $^{***}P < 0.001$, $^{****}P < 0.0001$.

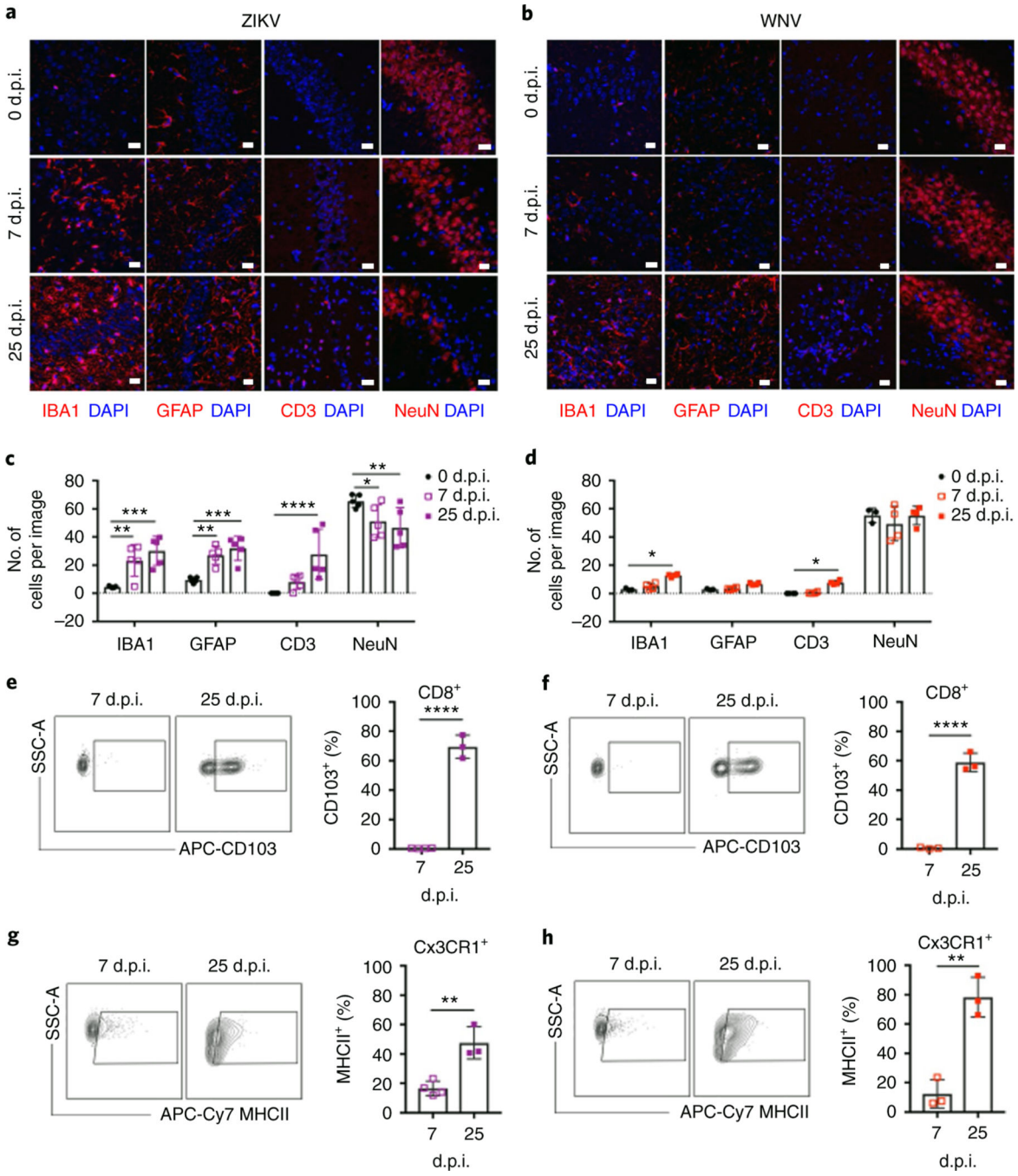

Fig. 2 |. ZiKV induces neuroinflammation and neuronal loss in the hippocampus.

a-d, ZIKV and WNV induce differential neuropathology in the hippocampus of WT mice. IHC analysis revealed that the number of microglia (IBA1$^+$), astrocytes (GFAP$^+$), and T cells (CD3$^+$) increases in the hippocampus after infection with either virus, but the number of neurons (NeuN$^+$) decreases following ZIKV infection. **a,b**, Representative images shown. Scale bars, 20 μm. **c,d**, The number of cells were quantified as indicated. For **c**, $n = 3$ (0 d.p.i.) or 5 (7, 25 d.p.i.) mice per group. IBA1, $P = 0.0051$ (0 versus 7d.p.i.) and $P = 0.0001$ (0 versus 25d.p.i.); GFAP, $P = 0.0086$ (0 versus 7d.p.i.) and $P = 0.0008$ (0 versus 25 d.p.i.);

CD3, $P = 0.0001$ (0 versus 25 d.p.i.); NeuN, $P = 0.0342$ (0 versus 7d.p.i.) and $P = 0.0046$ (0 versus 25 d.p.i.). For **d**, $n = 3$ (0,25) or 4 (7d.p.i.) mice per group. IBA1, $P = 0.0125$; CD3, $P = 0.0367$. **e-h**, T cells persist in the hippocampus after viral clearance, and microglia demonstrate persistent activation. Flow cytometry analysis of cells isolated from the hippocampus of $CC3CR1^{GFP}CCR2^{RFP}$ reporter animals at the indicated d.p.i. (gating strategy shown in Supplementary Fig 2). Data are representative of two independent experiments. **e,f**, ZIKV (**e**) and WNV (**f**) infection leads to increased expression of CD103 in $CD45^{hi}CD11b^{-}CD8^{+}$ T cells ($n = 3$ mice per group; $P<0.0001$). **g,h**, $CD45^{mid}CD11b^{+}Cx3CR1^{+}CCR2^{-}$ microglia isolated from the hippocampus of ZIKV-infected (**g**) and WNV-infected mice (**h**) express high levels of MHCII at 25 d.p.i. ($n = 3$ mice per group; $P = 0.0035$ (**g**) and $P = 0.0023$ (**h**)). For **c-h**, data represent the mean±s.d. and were analyzed by two-way ANOVA, corrected for multiple comparisons (**c** and **d**) or by unpaired two-sided *t*-test (**e-h**). $*P<0.05$, $**P< 0.005$, $***P< 0.001$, $****P< 0.0001$

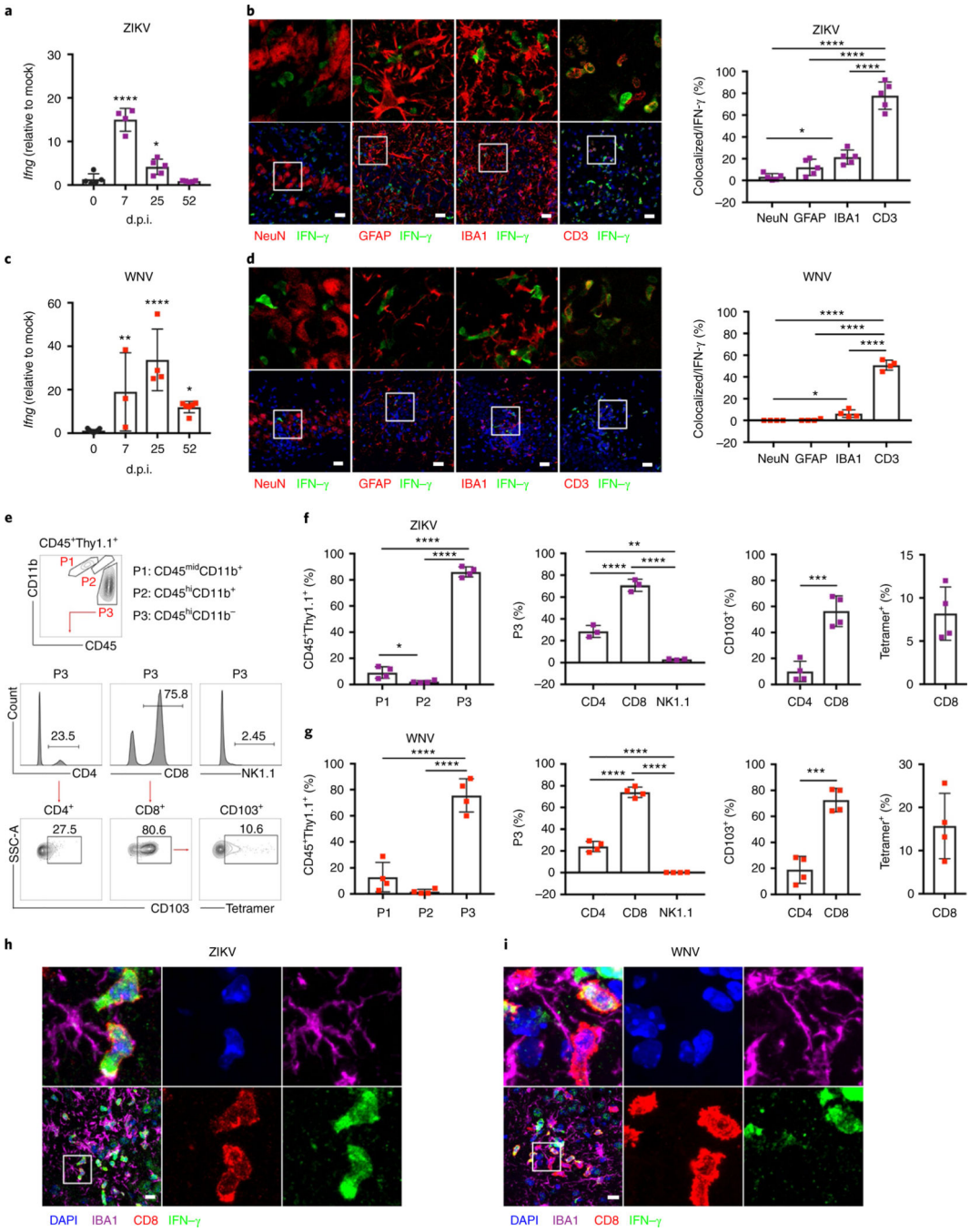

Fig. 3 |. T cells express IFN-γ in the post-infected hippocampus.

a,c, qPCR analysis of *Ifng* expression in the hippocampus at the indicated d.p.i. For **a**, $n = 4$ (0, 7 d.p.i.) or 5 (25, 52 d.p.i.) mice per group. For **c**, n = 4 (0, 25d.p.i.), 3 (7 d.p.i.), or 5 (52 d.p.i.) mice per group. For **a** (left to right), $P = 0.0001$ and $P = 0.0376$. For **c** (left to right), $P = 0.0021$, $P = 0.0001$, and $P = 0.0145$. **b-g**, IFN-γ is primarily expressed by $CD3^+CD8^+$ T cells at 25 d.p.i. **b,d**, Immunostaining (left) and quantitation (right) of hippocampi at 25d.p.i. from IFN-γ-YFP reporter mice for IFN-γ (YFP) and cell-type-specific markers for neurons (NeuN), astrocytes (GFAP), microglia (IBA1), and T cells (CD3) to identify the source of

IFN-γ in the hippocampi of infected mice post recovery. Images in the upper panel are magnifications of the boxed area in the corresponding images in the lower panel. Scale bars, 20 μm. For **b**, $n = 5$ mice per group; $P = 0.0143$ (NeuN versus GFAP) and $P < 0.0001$ (for other comparisons). For **d**, $n = 4$ mice per group; $P = 0.0439$ (NeuN versus GFAP) and $P < 0.0001$ (for other comparisons). **e-g**, $CD45^{+}IFN\text{-}\gamma^{+}$ cells isolated from the hippocampus of IFN-γ-Thy1.1 reporter mice at 25d.p.i. e, Gating strategy. Cells were gated via CD45 and CD11b to identify putative microglial (P1: $CD45^{mid}CD11b^{+}$), macrophage (P2: $CD45^{hi}CD11b^{+}$), and lymphocyte (P3: $CD45^{hi}CD11b^{-}$) populations among IFN-γ-expressing cells. Population P3 was further analyzed for CD4, CD8, and NK1.1 expression. IFN-$\gamma^{+}CD4^{+}$ and IFN-$\gamma^{+}CD8^{+}$ T cells were further analyzed for CD103 expression, and IFN-$\gamma^{+}CD8^{+}$ T cells were analyzed for virus specificity via NS4B tetramer staining. **f,g**, Quantification of indicated populations ($n = 4$ mice per group). For **f**, $P = 0.0402$ (P1 versus P2), $P < 0.0001$ (for other comparisons), $P = 0.0011$ (P3: CD4 versus CD8), and $P = 0.0006$ ($CD103^{+}$: CD4 versus CD8). For **g**, $P < 0.0001$ (for other comparisons) and $P = 0.0002$ ($CD103^{+}$: CD4 versus CD8). Full gating strategy and absolute numbers are provided in Supplementary Fig 3. **h,i**, IFN-$\gamma^{+}CD8^{+}$ T cells are closely associated with microglia in the post-infectious CNS. Representative immunostaining of the CA3 region of the hippocampus for IFN γ, CD8, IBA1, and DAPI. Data are representative of one independent experiment. For **a-d**, **f**, and **g**, data represent the mean±s.d. and were analyzed by one-way ANOVA and corrected for multiple comparisons. $^{*}P<0.05$, $^{**}P< 0.005$, $^{***}P<0.001$, $^{****}P<0.0001$.

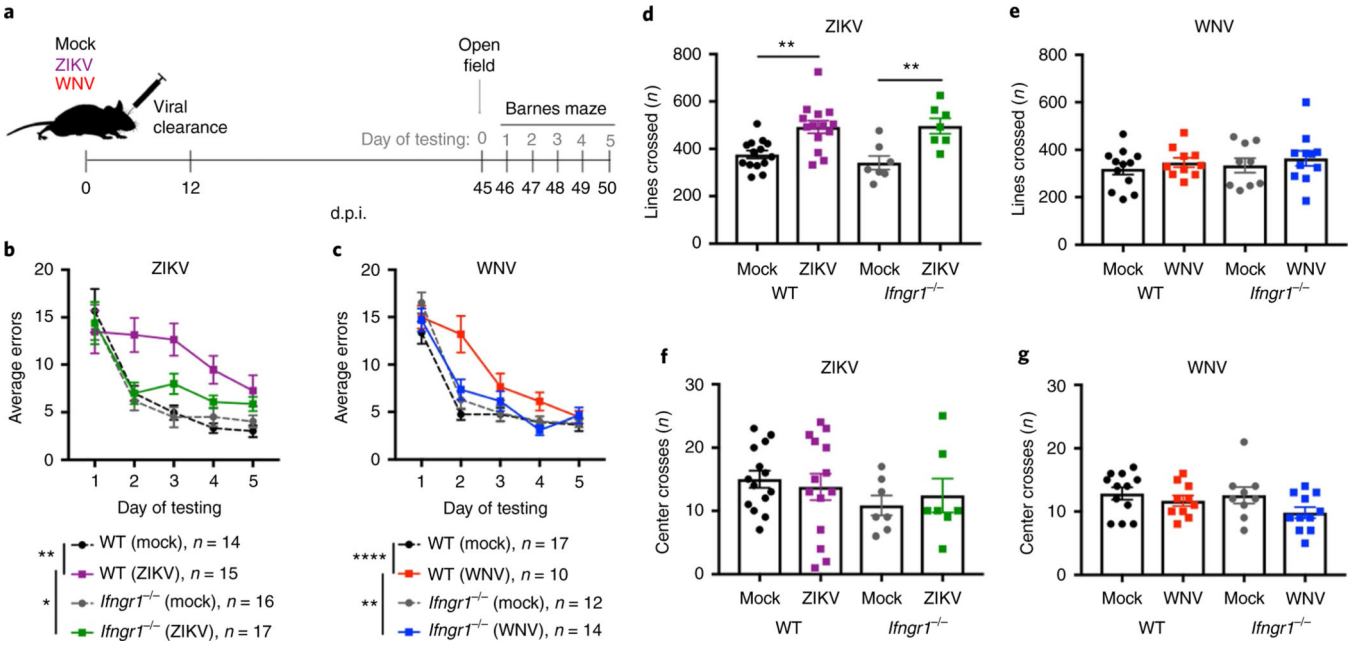

Fig. 4 |. Loss of IFN-γ signaling protects animals against spatial-learning deficits.

a-g, WT mice display spatial-learning deficits 1 month after viral clearance. *Ifngr1*$^{-/-}$ animals are protected against these deficits. Data were pooled from four independent experiments, with the sample size for each group indicated in **b** and **c. a**, Schematic of the model of viral infection and recovery. **b,c**, Average errors on the Barnes maze (sample sizes are indicated). For **b**, $P = 0.0012$ (WT mock versus ZIKV) and $P = 0.0381$ (*Ifngr1*$^{-/-}$ mock versus ZIKV). For **c**, $P<0{,}0001$ (WT mock versus ZIKV) and $P = 0.0186$ (*Ifngr1*$^{-/-}$ mock versus ZIKV). **d-g**, Open-field data to assess locomotor activity (lines crossed; **d,e**) and anxiety (center crosses; **f,g**) in 5 min when exploring an open-field arena (for sample sizes, see the corresponding colors in **b** and **c**). For **d** (left to right), $P = 0.0032$ and $P = 0.0059$. For **b-g**, data represent the mean±s.e.m. and were analyzed by two-way ANOVA, and corrected for multiple comparisons. *$P<0.05$, **$P< 0.005$, ****$P< 0.0001$.

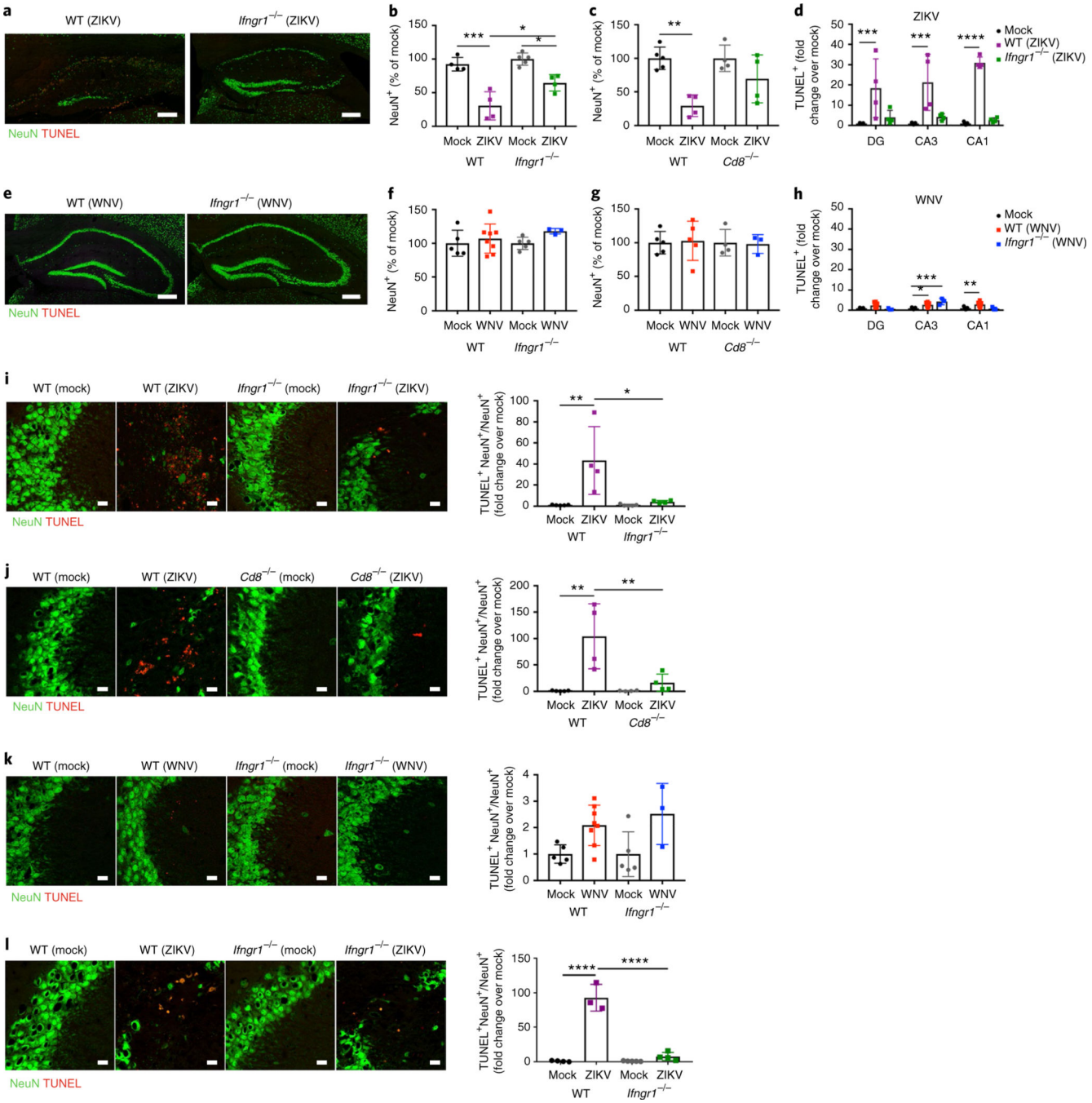

Fig. 5 |. IFN-γ promotes neuronal apoptosis in ZiKV-infected animals post recovery.

a-h, ZIKV, but not WNV, infection leads to decreased numbers of hippocampal neurons at 25 d.p.i. More neurons were found in infected *Ifngr1*$^{-/-}$ and *Cd8*$^{-/-}$ mice post recovery. **a-c,e-g**, Representative images (**a**,e) and quantitation (b,c,f,g) of neurons in the hippocampus. Data were pooled from two to three independent experiments. For b, $n = 4$ (WT mock, WT ZIKV, *Ifngr1*$^{-/-}$ ZIKV) or 5 (*Ifngr7*$^{-/-}$ mock) mice per group. For **c**, $n = 5$ (WT mock) or 4 (WT ZIKV, *Ifngr1*$^{-/-}$ mock, *Ifngr1*$^{-/-}$ ZIKV) mice per group. For **f**, $n = 5$ (WT mock, *Ifngr7*$^{-/-}$ mock), 7 (WT WNV), or 3 (*Ifngr1*$^{-/-}$ ZIKV) mice per group. For **g**, $n = 5$ (WT

mock, WT ZIKV), 4 (*Ifngrl*$^{-/-}$ mock), or 3 (*Ifngrl*$^{-/-}$ ZIKV) mice per group. For **b** (left to right), *P*= 0.001, *P*= 0.0111, and ***P*** = 0.0214. For **c**, *P*= 0.0032. Scale bars, 200μm. **d,h**, Quantitation of TUNEL^{+} cells in multiple regions of the hippocampus at 25 d.p.i. following ZIKV and WNV infection of WT and *Ifngrl*$^{-/-}$ mice. Note that levels of apoptosis were much lower in WNV-infected animals post recovery. Data were pooled from two independent experiments (*n* = 4 mice per group). For **d** (left to right), *P* = 0.0009, *P = 0.0001,* and *P = 0.0001.* For **h** (left to right), *P* = 0.0138, *P* = 0.0002, and *P* = 0.0068. **i,j**, ZIKV infection leads to significant increases in TUNEL^{+}NeuN^{+} cells, which is not observed in *Ifngrl*$^{-/-}$ or *Cd8*$^{-/-}$ mice post recovery. Data were pooled from two independent experiments. For **i**, *n* = 5 mice per group; *P* = 0.0049 and *P* = 0.0134 (left to right). For **j**, *n* = 4 mice per group; *P* = 0.0014 and *P* = 0.0081 (left to right). **k**, Quantitation of TUNEL $^{+}$NeuN^{+} cells at 25 d.p.i. with WNV. Data were pooled from two independent experiments (*n* = 5 (WT mock, *Ifngrl*$^{-/-}$ mock), 7 (WT WNV), or 3 (*Ifngrl*$^{-/-}$ WNV) mice per group). l, Quantitation of TUNEL^{+}NeuN^{+} in ZIKV-infected WT versus *Ifngrl*$^{-/-}$ mice at 52d.p.i. Data were pooled from two independent experiments (*n* = 4 mice per group; *P*< 0.0001). Scale bars, 20 μm. For **b-d**, **f-l**, data represent the mean±s.d. and were analyzed by two-way ANOVA, and corrected for multiple comparisons (**b-h**). **P*<0.05, ***P*<0.005, ****P*<0.001

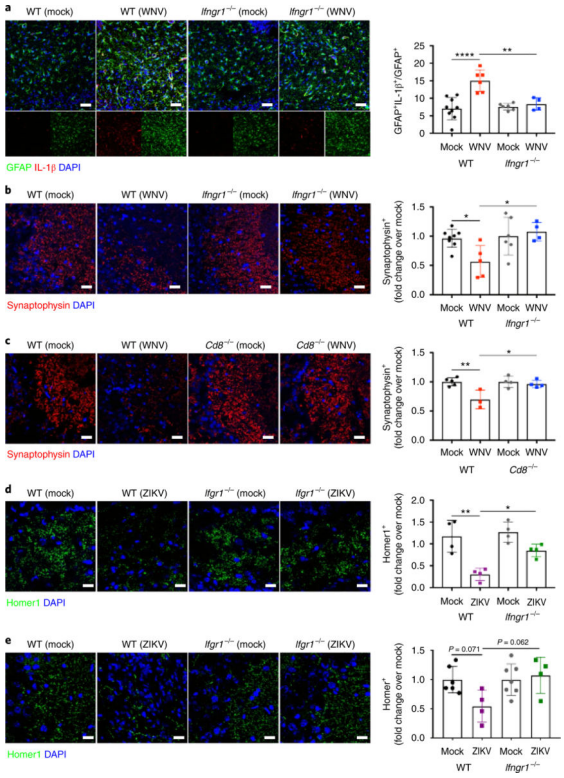

Fig. 6 |. iFNGR is required for repair of presynaptic and postsynaptic termini in flavivirus-infected animals post recovery.

a-c, WNV infection induces astrocyte IL-1β production, which leads to delayed recovery of synapses in the hippocampus at 25 d.p.i. in WT mice, but *Ifngrl*$^{-/-}$ and *Cd8*$^{-/-}$ animals display early recovery of presynaptic termini. **a**, Representative immunostaining (left) and quantitation (right) of the hippocampus. Data were pooled from three independent experiments (n = 9 (WT mock), 6 (WT WNV, *Ifngrl*$^{-/-}$ mock), or 4 (*Ifngrl*$^{-/-}$ WNV) mice per group; P<0.0001 (left) and P= 0.0040 (right)). Scale bar, 50 μm. **b,c**, Representative immunostaining (left) and quantitation (right) of the hippocampus at 25d.p.i. Data were pooled from three independent experiments. For **b**, n = 9 (WT mock), 6 (WT WNV, *Ifngrl*$^{-/-}$ mock), or 4 (*Ifngrl*$^{-/-}$ WNV) mice per group; P = 0.0311 (left) and P = 0.0169 (right). For **c**, n = 5 (WT mock), 3 (WT WNV), or 4 (*Ifngrl*$^{-/-}$ Mock, *Ifngrl*$^{-/-}$ WNV) mice per group; P = 0.0048 (left) and P = 0.0157 (right). Scale bars, 50 μm. **d,e**, ZIKV infection leads to chronic loss of Homer1^{+} postsynaptic terminals at 25 and 52 d.p.i. in WT mice, but *Ifngrl*$^{-/-}$ animals display recovery. **d**, Representative immunostaining (left) and quantitation (right) of the hippocampus at 25d.p.i. Data were pooled from two independent experiments (n = 4 mice per group; P= 0.0011 (left) and P = 0.0311 (right)). Scale bar, 10μm. **e**, Representative immunostaining (left) and quantitation (right) of the hippocampus at 52 d.p.i. Data were pooled from two independent experiments (n = 6 (WT mock), 4 (WT WNV, *Ifngrl*$^{-/-}$ WNV), or 7 (*Ifngrl*$^{-/-}$ Mock) mice per group). Scale bar, 10 μm. For all panels, data represent the mean±s.d. and were analyzed by two-way ANOVA, and corrected for multiple comparisons. *P<0.05, **P<0.005, ****P<0.0001.

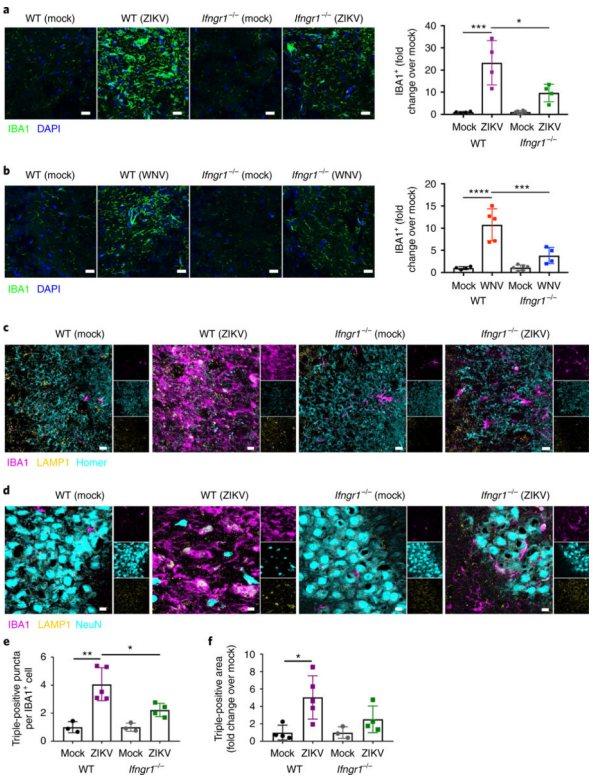

Fig. 7 |. IFN-γ potentiates microglial engulfment of postsynaptic termini and neurons in ZiKV-infected animals post recovery.

a,b, WNV or ZIKV infection induces increased expression of IBA1 in the hippocampus at 25d.p.i., which is significantly reduced in *Ifngr1*$^{-/-}$ mice. Representative immunostaining (left) and quantitation (right) of the hippocampus at 25d.p.i. Data were pooled from two independent experiments. For **a**, $n = 4$ mice per group; P=0.0001 (left) and $P = 0.0102$ (right). For **b**, $n = 4$ (WT mock, WT WNV, *Ifngr1*$^{-/-}$ WNV) or 6 (*Ifngr1*$^{-/-}$ mock) mice per group; $P < 0.0001$ (left) and $P = 0.0010$ (right). Scale bars, 50 μm. c,e, IBA1^{+} microglia engulf postsynaptic termini at 25d.p.i., which is significantly reduced in *Ifngr1*$^{-/-}$ mice. Representative immunostaining, with single-channel images on the right (**c**) and quantitation (**e**) of the hippocampus of infected mice post recovery. Data were pooled from two independent experiments ($n = 3$ (WT Mock, *Ifngr1*$^{-/-}$ Mock), 5 (WT ZIKV), or 4 (*Ifngr1*$^{-/-}$ ZIKV) mice per group; P= 0.0011 (left) and $P = 0.0209$ (right)). Scale bars, 10 μm. **d,f**, IBA1^{+} microglia engulf NeuN^{+} perikarya at 25d.p.i., which is reduced in *Ifngr1*$^{-/-}$ mice. Representative immunostaining, with single-channel images on the right (**d**) and quantitation (**f**) of the hippocampus of infected mice post recovery. Data were pooled from two independent experiments ($n = 4$ (WT Mock, *Ifngr1*$^{-/-}$ ZIKV), 5 (n = WT ZIKV), or 3 (*Ifngr1*$^{-/-}$ Mock) mice per group; $P = 0.0190$). Scale bars, 10μm. For **a, b, e**, and **f**, data represent the mean±s.d. and were analyzed by two-way ANOVA, corrected for multiple comparisons. *P<0.05, ***P< 0.001, ****P< 0.0001.

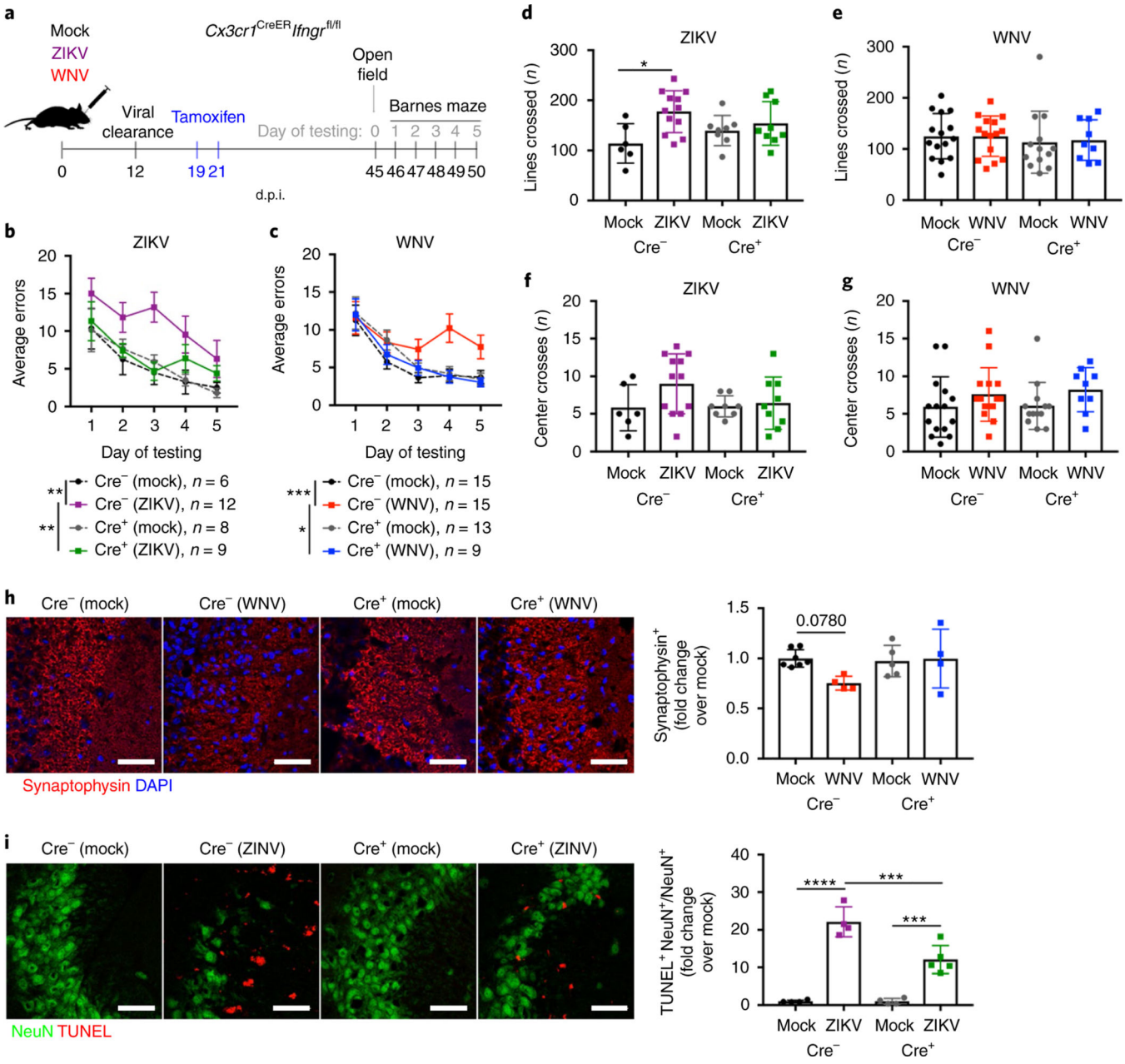

Fig. 8 |. Loss of IFN-γ signaling in microglia during recovery protects animals against spatial-learning deficits.

a-g, Specific deletion of IFNGR in microglia after viral clearance is sufficient to protect animals against WNV-or ZIKV-induced spatial-learning deficits. **a**, Experimental design. *Cx3cr1*^{CreER}*Ifngr*$^{fl/fl}$ (Cre^{+}) animals were generated, and *Cx3cr1*^{CreER}*Ifngr*$^{fl/fl}$ (Cre^{-}) littermates were used as controls. Mice were challenged intracranially with mock, WNV, or ZIKV at 8 weeks of age. All mice were treated with tamoxifen at 19 and 21 d.p.i. to induce Cre-recombinase expression and achieve deletion of *Ifngr* in CX3CR1^{+} microglia. Behavioral testing began on 45 d.p.i. with OFTs, followed by 5 consecutive days of Barnes maze testing. **b,c**, Average errors on the Barnes maze. Data were pooled from four independent experiments, and sample sizes are as listed. For **b**, P= 0.0011 (Cre^{-} mock and

ZIKV) and $P = 0.0073$ (Cre^+ mock and ZIKV). For **c**, $P = 0.003$ (Cre^- mock and ZIKV) and $P = 0.0207$ (Cre^+ mock and ZIKV). **d-g**, OFT data to assess locomotor activity (lines crossed; **d,e**) and anxiety (center crosses; **e,g**) in 5 min when exploring an open-field arena. Data were pooled from four independent experiments (for sample sizes, see the corresponding colors in **b** and **c**); $P = 0.0146$ (**d**). **h,i**, Specific deletion of *Ifngr* in microglia after viral clearance is sufficient to protect animals against WNV-or ZIKV-mediated synapse and neuronal loss, respectively. Cre^+ and Cre^- littermates were infected with mock, WNV, or ZIKV and treated with tamoxifen as described above, but tissue was collected at 25 d.p.i. for IHC analysis of synaptophysin or NeuN and TUNEL positivity. Data were pooled from two independent experiments. For **h**, $n = 7$ (Cre^- Mock), 4 (Cre^- WNV, Cre^+ WNV), or 5 (mock Cre^+) mice per group. For **i**, n = 4 (Cre^- mock, Cre^- ZIKV, Cre^+ mock) or 5 (Cre^+ ZIKV) mice per group. Scale bars, 20 μm. Data represent the mean±s.e.m. (**b** and **c**) or mean±s.d. (**d-i**) and were analyzed by two-way ANOVA, and corrected for multiple comparisons (**a-i**). $*P<0.05$, $**P< 0.005$, $***P< 0.001$, $****P< 0.0001$.